Gordon Research Conference 2009: Coastal Ocean Circulation

Anisotropic response of surface currents to the wind in a coastal region

Sung Yong Kim†, Bruce D. Cornuelle, and Eric J. Terrill

Scripps Institution of Oceanography, La Jolla, CA 92093-0213

syongkim@ucsd.edu†

Abstract

Analysis of coastal surface currents measured off the coast of San Diego for two years suggests an anisotropic and asymmetric response to the wind, probably as a result of bottom/coastline boundary effects including pressure gradients. In a linear regression, the statistically estimated anisotropic response explains approximately 20% more surface current variance than an isotropic wind-ocean response model. After steady wind forcing for three days, the isotropic surface current response veers 42°±2° to the right of the wind regardless of wind direction, whereas the anisotropic analysis suggests that the upcoast (onshore) wind stress generates surface currents with 10°±4° (71°±3°) to the right of the wind direction. The anisotropic response thus reflects the dominance of alongshore currents in this coastal region. Both analyses yield wind-driven currents with 3%–5% of the wind speed, as expected. In addition, nonlinear isotropic and anisotropic response functions are considered, and the asymmetric current responses to the wind are examined. These results provide a comprehensive statistical model of the wind-driven currents in the coastal region, which has not been well identified in previous field studies, but is qualitatively consistent with descriptions of the current response in coastal ocean models.

1 Theoretical background

Adjustment terms (A_x and A_y) in the momentum equations are introduced that are only related to the wind-driven currents modeling both bottom drag and pressure gradient set up along the coast:

$$\frac{\partial u}{\partial t} - f_c v + A_x = \frac{1}{\rho}\frac{\partial}{\partial z}\left(\mu \frac{\partial u}{\partial z}\right), \quad (1)$$

$$\frac{\partial v}{\partial t} + f_c u + A_y = \frac{1}{\rho}\frac{\partial}{\partial z}\left(\mu \frac{\partial v}{\partial z}\right), \quad (2)$$

where f_c, ρ, and μ denote the Coriolis frequency, the seawater density, and the dynamic viscosity, respectively. The depth coordinate (upward positive) is denoted as z.

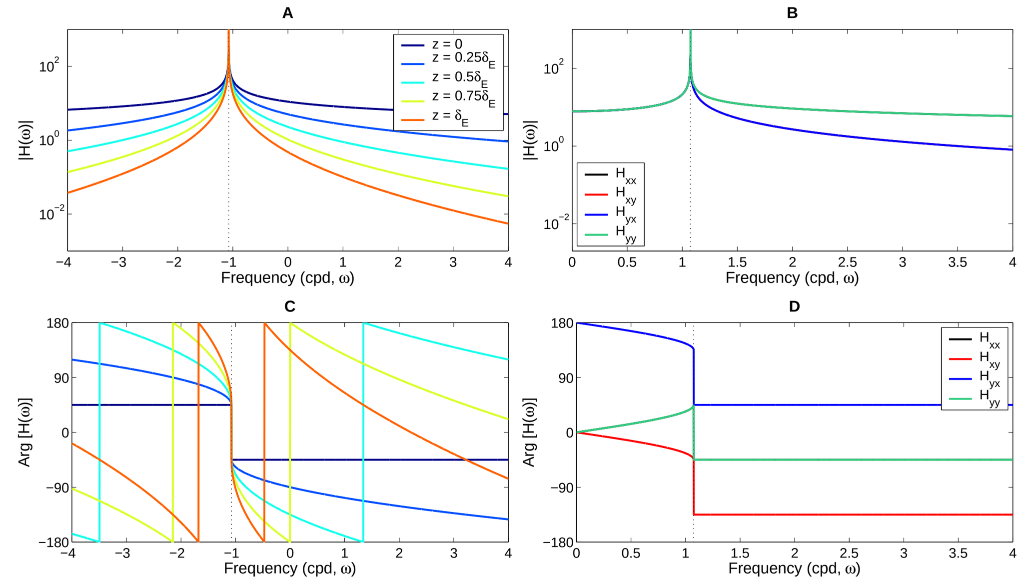

Figure 1: (a),(c) The magnitude and phase of the linear isotropic transfer function in the Ekman theory [1, 2] at each 0.25δ_E depth increment from the surface ($z = 0$) to the Ekman depth ($z = \delta_E$). (b),(d) The magnitude and phase of the four functions of the linear anisotropic transfer function at the surface for a parameter choice as the Ekman theory. The isotropic/anisotropic transfer functions are calculated assuming infinite water depth with depth-independent viscosity ($\nu = 1 \times 10^{-4}$ $\mathrm{m^2\,s^{-1}}$) and no friction ($r_{xx} = 0$ and r_{yy} = 0). The terms H_{xx} and H_{yy} in (b) and (d) are superposed, and H_{xy} and H_{yx} in (b) are superposed. The vertical dotted line indicates the inertial frequency ($\omega = \pm 1.07$ cpd) in the study domain.

Assuming μ is independent of depth, the adjustment terms are composed of pressure gradients and the anisotropic part of the stress divergence:

$$A_x = \frac{1}{\rho}\frac{\partial p}{\partial x} - \nu_a \frac{\partial^2 u}{\partial z^2}, \quad (3)$$

$$A_y = \frac{1}{\rho}\frac{\partial p}{\partial y} - \nu_a \frac{\partial^2 v}{\partial z^2}, \quad (4)$$

where ν and ν_a denote the isotropic and anisotropic kinematic viscosity, respectively.

For the statistical analysis on the observations, the adjustment terms are considered as convolutions of the time history of currents:

$$A_x = a_{xx} * u + a_{xy} * v = \int_{-\infty}^{\infty} a_{xx}(\xi) u(t-\xi) + a_{xy}(\xi) v(t-\xi)\, \mathrm{d}\xi, \quad (5)$$

$$A_y = a_{yx} * u + a_{yy} * v = \int_{-\infty}^{\infty} a_{yx}(\xi) u(t-\xi) + a_{yy}(\xi) v(t-\xi)\, \mathrm{d}\xi, \quad (6)$$

where a_{xx}, a_{xy}, a_{yx}, and a_{yy} represent the effects of the bottom and coastline boundary friction and the pressure gradient set up near the coast. They are convolved in the time domain with the current components (u and v) in the x and y directions, respectively (The asterisk is the time domain convolution operator).

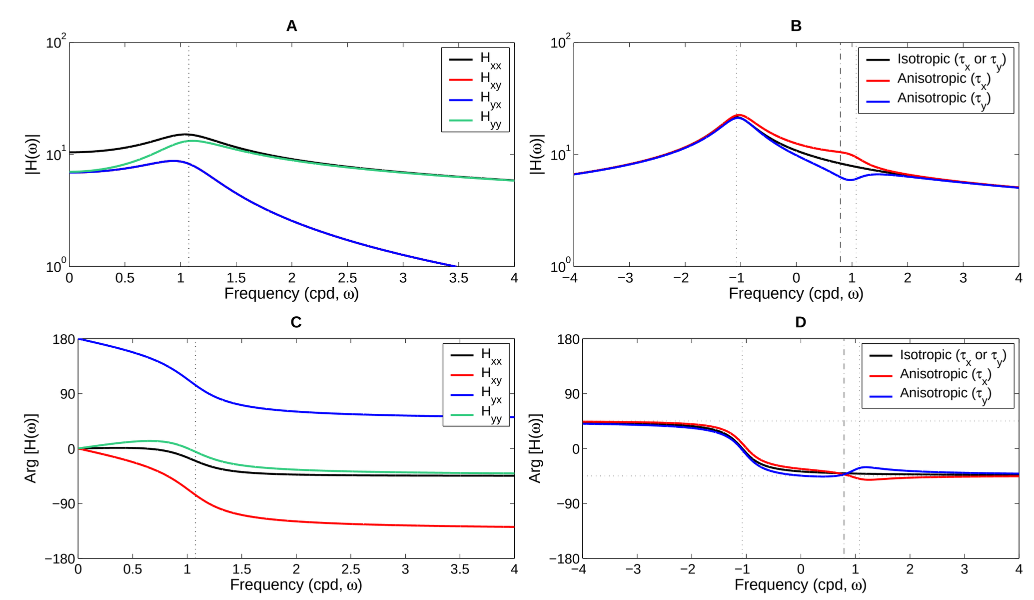

Figure 2: The linear anisotropic transfer function based on the extended Ekman theory with depth-independent viscosity ($\nu = 1 \times 10^{-4}$ $\mathrm{m^2\,s^{-1}}$) and two different frictions in the x and y directions ($r_{xx} = 1 \times 10^{-6}$ $\mathrm{s^{-1}}$ and $r_{yy} = 4 \times 10^{-5}\,\mathrm{s^{-1}}$). (a) The magnitude of the anisotropic transfer function. (b) The magnitude of the isotropic transfer function with same viscosity and the friction as the arithmetic mean of two frictions [$r = (r_{xx} + r_{yy})/2$], and the magnitude of the anisotropic transfer function when wind stress (τ_x or τ_y) is applied in each direction. (c) The phase of the anisotropic transfer function. (d) The phase of the isotropic/anisotropic transfer functions. The phase transition frequency (ω_0) is 0.7909 cpd [a vertical dash-dotted line in (b) and (d)] for the selected parameters. The terms H_{xy} and H_{yx} in (a) are overlapped. See Fig. 1 for definition of the vertical dotted line.

2 Observations

Surface currents used for this study were observed by high-frequency (HF; ∼25 MHz) radars for two years (April 2003–March 2005) over a 40 km region from the coast of southern San Diego County ([3]). The wind observed at Tijuana River (Tidal Linkage station, Fig. 3) during the same period as the surface current is hourly averaged.

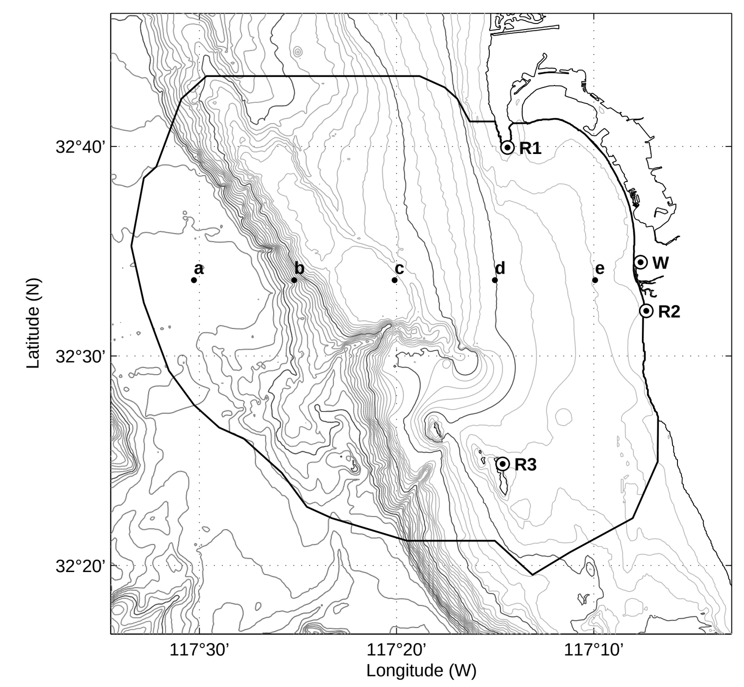

Figure 3: The study domain of surface currents and the wind. The effective spatial coverage area where the HF radars (R1, R2, and R3) observed is indicated with black curve. Three HF radar sites are Point Loma (R1), Border Park (R2), and Coronado Island (R3). The Tijuana River wind station (W) is located near the Tijuana River valley. The bottom bathymetry contours are indicated by the thin curves with 10 m ($0 < z < 100$ m) and 50 m ($100 < z < 1000$ m) contour intervals and the thick curves at the 50, 100, 500, and 1000-m depths.

3 Methods

3.1 Frequency domain

The linear regression equation in the frequency domain is

$$\hat{\mathbf{u}}(z,\omega) = \mathbf{H}(z,\omega)\hat{\boldsymbol{\tau}}(\omega). \quad (7)$$

The transfer function ($\mathbf{H}$) is computed from the (time) ensemble covariance average of the Fourier coefficients of surface currents ($\hat{\mathbf{u}}$) and wind stress ($\hat{\boldsymbol{\tau}}$) at each frequency (ω):

$$\mathbf{H}(z,\omega) = \left[\langle \hat{\mathbf{u}}(z,\omega)\, \hat{\boldsymbol{\tau}}^{\dagger}(\omega)\rangle\right] \left[\langle \hat{\boldsymbol{\tau}}(\omega)\, \hat{\boldsymbol{\tau}}^{\dagger}(\omega)\rangle + \mathbf{R_a}\right]^{-1}, \quad (8)$$

where † indicates the complex conjugate transpose, $\langle\cdot\rangle$ is the ensemble average, and $\mathbf{R_a}$ is the regularization matrix and is assumed to be the noise level of the wind stress.

3.2 Time domain

The covariance of currents and wind stress is

$$\langle \mathbf{u}\boldsymbol{\tau}^\dagger\rangle = \int_{t'} \mathbf{g}(z, t-t')\, \langle \boldsymbol{\tau}(t')\boldsymbol{\tau}(t)^\dagger\rangle\, \mathrm{d}t' \quad (9)$$

and is truncated and discretized as a finite sum:

$$\langle \mathbf{u}\boldsymbol{\tau}^\dagger\rangle = \sum_{k=0}^{N} \mathbf{g}(z, k\Delta t)\, \langle \boldsymbol{\tau}(t-k\Delta t)\boldsymbol{\tau}(t)^\dagger\rangle. \quad (10)$$

In other words,

$$\langle \mathbf{u}(z,t)\, \boldsymbol{\tau}_N^\dagger(t)\rangle = \mathbf{G}(z)\langle \boldsymbol{\tau}_N(t)\, \boldsymbol{\tau}_N^\dagger(t)\rangle, \quad (11)$$

where $\boldsymbol{\tau}_N(t) = [\boldsymbol{\tau}(t-N\Delta t) \cdots \boldsymbol{\tau}(t-\Delta t)\, \boldsymbol{\tau}(t)]^\dagger$ is the wind stress stacked with N hours time lag.

The response function ($\mathbf{G}$) is computed from the covariance matrix between surface currents ($\mathbf{u}$) and time lag wind stress ($\boldsymbol{\tau}_N$):

$$\mathbf{G}(z) = \left[\langle \mathbf{u}(z,t)\, \boldsymbol{\tau}_N^\dagger(t)\rangle\right] \left[\langle \boldsymbol{\tau}_N(t)\, \boldsymbol{\tau}_N^\dagger(t)\rangle + \mathbf{R_b}\right]^{-1}, \quad (12)$$

where $\mathbf{G} = [\mathbf{g}_1\, \mathbf{g}_2 \cdots \mathbf{g}_N]^\dagger$, and $\mathbf{R_b}$ is the regularization matrix, which compensates for the sample error in the covariance matrix by suppressing small or negative eigenvalues.

4 Results

4.1 Transfer functions

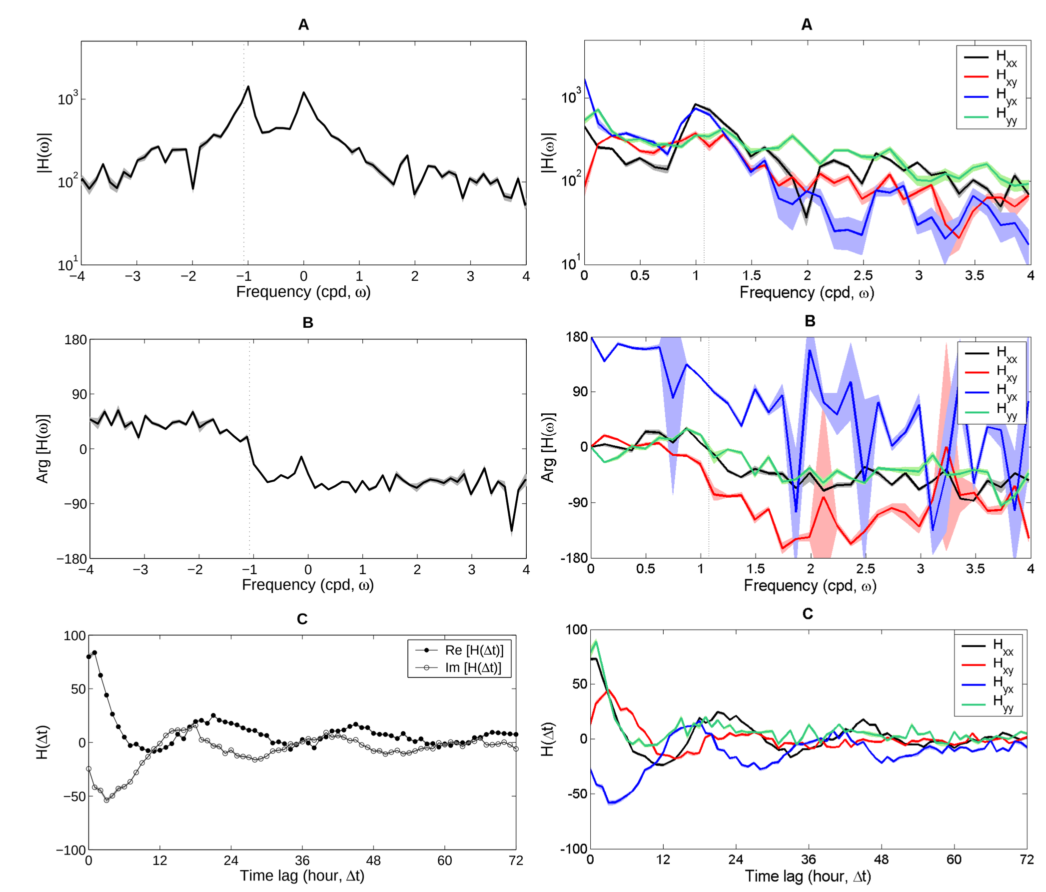

Figure 4: (left) Isotropic transfer function. (right) Anisotropic transfer function. (a) Magnitude, (b) phase, and (c) temporal amplitudes of the linearly estimated WIRF. The isotropic transfer function is estimated with 90 subsamples. The uncertainty shown as the gray-shaded region in (a) and (b) is calculated from 30 realizations using the jackknife method. The vertical dot line indicates the inertial frequency ($\omega = -1.07$ cpd) in the study domain.

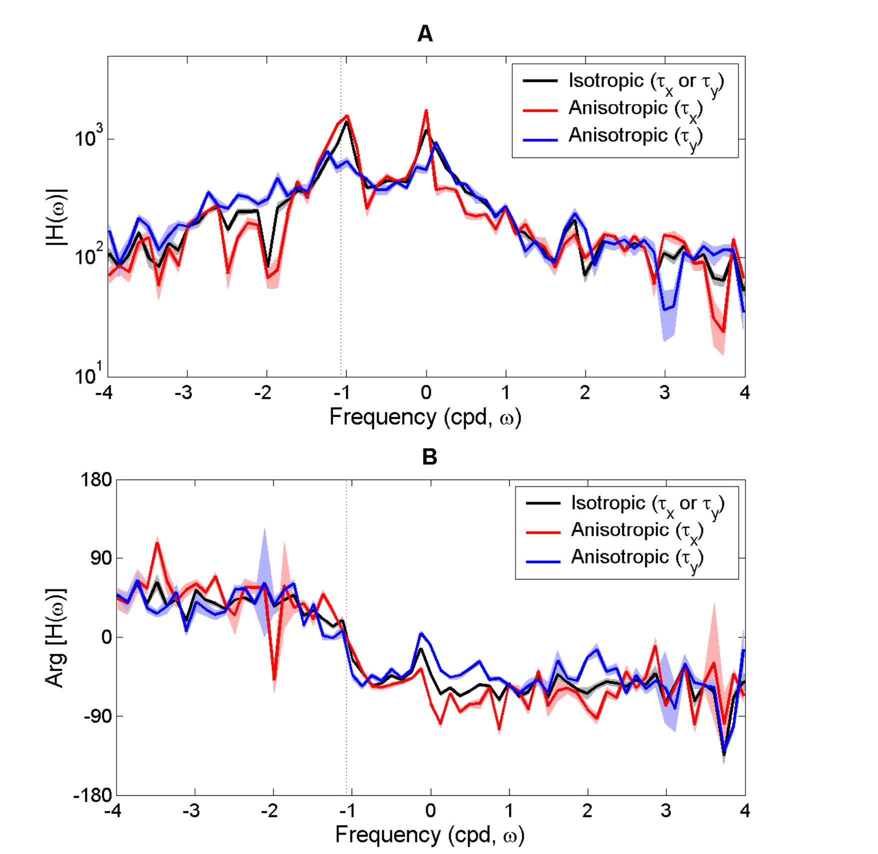

Figure 5: (a) Magnitude and (b) phase of the linearly estimated isotropic/anisotropic transfer functions for wind stress (τ_x and τ_y), respectively. The phase of the anisotropic transfer function for the y-directional wind stress (τ_y) is shifted down by 90° to align with the others. The solid curves in (a) and (b) are the same as in Figs. 4a and 4b, respectively. See Fig. 4 for the definition of the vertical dotted line.

4.2 Time integrations

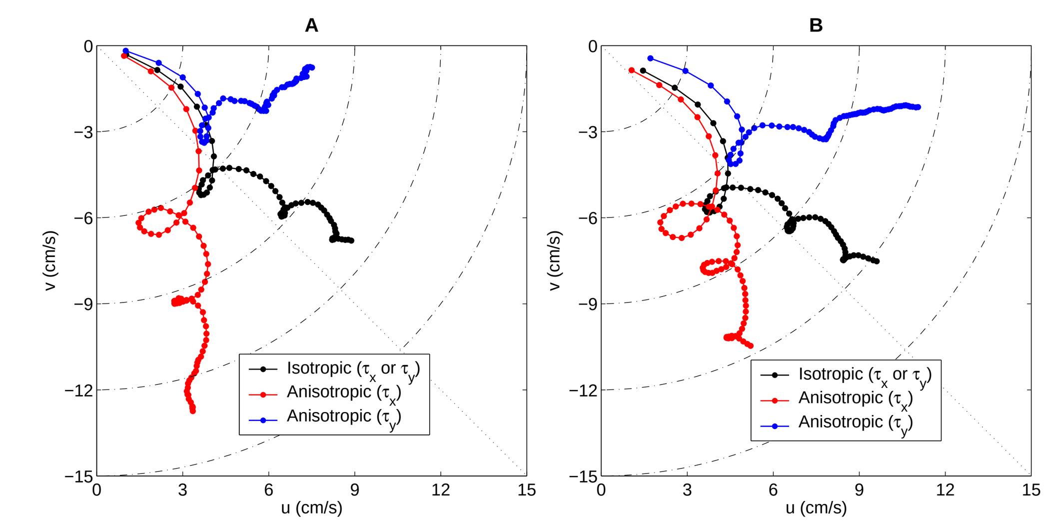

Figure 6: Time integrations of the temporal amplitudes of the linearly estimated transfer functions for a constant wind stress during three days for (a) isotropic/anisotropic transfer functions and (b) isotropic/anisotropic response functions. The wind stress at either direction (τ_x or τ_y) of the typical wind speed ($|\mathbf{u}| = 3\ \mathrm{m\,s^{-1}}$) in the study domain is applied. Anisotropic response for the y-directional wind stress (τ_y) is rotated 90° clockwise to align with other responses. The thin dashdotted quarter-circular curves denote the percentage of the wind-driven current speed to the wind speed, which are 1%, 2%, 3%, 4%, and 5% from the origin, and the thin dotted line indicates the direction of 45° to the right of the wind stress.

Acknowledgment

Authors are supported by the COCMP, ONR, NOAA. Surface current data are provided from the Southern California Coastal Ocean Observing System (SCCOOS, Available online at `http://www.sccoos.org`) at SIO, and wind data at Tijuana River (Tidal Linkage) are maintained by the System-Wide Monitoring Program at the TRNERR, CDMO (Available online at `http://cdmo.baruch.sc.edu/`). We thank M. Otero, L. Hazard, P. Reuter, J. Bowen, and T. Cook in Coastal Observing Research and Development Center (CORDC, available online at `http://cordc.ucsd.edu/`) at SIO, and M. Ide, M. Cordrey, and J. Crook in TRNERR.

References

[1] V. W. Ekman, "On the influence of the Earth's rotation on ocean-currents," *Ark. Mat. Astron. Fys.*, vol. 2, pp. 1–53, 1905.

[2] J. Gonella, "A rotary-component method for analysis in meteorological and oceanographic vector time series," *Deep Sea Res.*, vol. 19, pp. 833–846, 1972.

[3] S. Y. Kim, E. J. Terrill, and B. D. Cornuelle, "Mapping surface currents from HF radar radial velocity measurements using optimal interpolation," *J. Geophys. Res.*, vol. 113, 2008, C10023, doi:10.1029/2007JC004244.